$Z_2 \times Z_2$ symmetry and Z_4 Berry phase of bosonic ladders

Yoshihito Kuno [1] and Yasuhiro Hatsugai [2]
[1]*Graduate School of Engineering Science, Akita University, Akita 010-8502, Japan*
[2]*Department of Physics, University of Tsukuba, Tsukuba, Ibaraki 305-8571, Japan*

(Received 21 April 2023; accepted 10 July 2023; published 27 July 2023)

Bose gas on a two-leg ladder exhibits an interesting topological phase. We show the presence of a bosonic symmetry-protected-topological (SPT) phase protected by $Z_2 \times Z_2$ symmetry. This symmetry leads to Z_4 fractional quantization of the Z_4 Berry phase, which is a topological order parameter to identify the bulk. Using the Z_4 Berry phase, we show that the interacting bosonic system possesses rich topological phases depending on the particle density and strength of interaction. Based on the bulk-edge correspondence, each edge state of the SPT phases is discussed in relation to the Z_4 Berry phases. In particular, we have found an intermediate phase that is not adiabatically connected to a simple adiabatic limit that possesses unconventional edge states, which we numerically demonstrate by employing the density-matrix renormalization-group algorithm.

DOI: 10.1103/PhysRevA.108.013319

I. INTRODUCTION

Synthetic dimension in a cold-atom system constituted by internal states of the atom offers a promising platform on which to simulate and investigate various states of matter [1]. An interesting lattice model has already been implemented, that is, a two- or three-leg ladder system with an artificial gauge field [2–7]. In cold-atom experiments, interacting systems can be implemented and their strength can be controllable [8], e.g., Feshbach resonance and using dipole-dipole interactions between dipolar atoms [9,10]. In particular, such a system with a specific lattice geometry can be used as a quantum simulator to realize rich topological states of matter.

In condensed-matter theory, the symmetry-protected-topological (SPT) phase is now an attractive state as one of topological states of matter [11]. So far, various types of SPT phases have been discovered and also a classification of the SPT phases has been proposed for some groups of systems. The classification for free-fermion systems has been explicitly given [12–14] (now called the tenfold way) and also for interacting bosonic systems. This is listed as a catalog of (bosonic) SPT phases by group cohomology [15,16]. These classification schemes showed possible SPT phases, but a demonstration of concrete examples in realistic systems is an ongoing problem. In this work we propose a specific concrete example of an interacting bosonic SPT phase of a two-leg ladder system, which is feasible in real experiments.

We consider a Bose-Hubbard model with two internal states of atoms, which can be regarded as a two-leg ladder system. Its experimental realization may be easier than that of a fermionic one since the temperature of the fermionic system in an optical lattice is somewhat high and it is still a challenging problem to observe a complete quantum long-range order, such as magnetization [17]. We assume that the bosonic model on the two-leg ladder includes on-site and vertical link interactions (interactions between two different internal states) and also a hopping dimerization. Then a specific type of bosonic interacting SPT phase appears, characterized by fractional quantization of the Z_4 Berry phase. Due to the two-leg ladder geometry, the system has a key symmetry to induce the SPT phase.

We find that the key symmetry is of the $Z_2 \times Z_2$ type, which consists of two types of reflection symmetry combined with time reversal (complex conjugation). In this work we show that the Z_N Berry phase [18–32] can be used as a topological order parameter to characterize the bosonic SPT phase. The Z_N Berry phase allows identifying rich topological phases and is applicable to both noninteracting and interacting systems, which is especially efficient for interacting bosonic systems. We analytically show that the Z_4 Berry phase is fractionally quantized by the presence of the $Z_2^* \times Z_2^*$ equivalence, as $\gamma = 2\pi n/4 \,\mathrm{mod} 2\pi$ $(n = 1, 2, 3, 4)$. The quantization is protected as long as the gap is open, even under a local twist with the symmetry constraints. If the state is adiabatically connected to a set of simple local clusters (a plaquette), we may expect the ground state is short-range entangled and topological properties are reduced to those of the simple one, that is, we can determine the distinct value n of the Z_4 Berry phase. In this work we numerically demonstrate the presence of the interacting bosonic SPT phases characterized by the fractional quantization of the Z_4 Berry phase coming from the $Z_2^* \times Z_2^*$ equivalence. Due to the Bose-Hubbard nature, we find rich SPT phases depending on the mean density and strength of interaction. Furthermore, a reduction of the equivalence $Z_2^* \times Z_2^* \to Z_2^*$ is demonstrated by the quantized Berry phases of $Z_4 \to Z_2$. Also, an eccentric intermediate phase, which is not adiabatically connected to the simple clusters, is demonstrated.

In relation to the Berry phase of the bulk SPT phase, we numerically discuss edge states based on the bulk-edge correspondence by using the density-matrix renormalization-group (DMRG) algorithm. We will show some case studies. Depending on the type of edges, mean density, and chemical potential, the density profile around the edges significantly varies, which indicates the appearance of unconventional edge states. In particular, we numerically find the clear edge density profile,

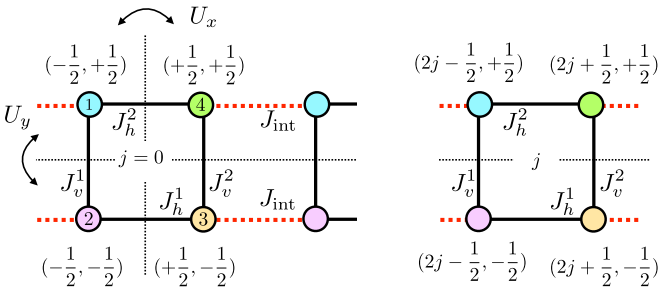

FIG. 1. Labeling of the sites and the lattice structure of the model with periodic boundary condition. Symmetry axes associated with the reflections U_x and U_y are also shown. Note that the open system by cutting the link at the origin [$J_h = 0$ at the $(-\frac{1}{2},\pm\frac{1}{2})$-$(+\frac{1}{2},\pm\frac{1}{2})$ links] also respects these symmetries, which guarantees the bulk-edge correspondence associated with the Z_4 Berry phase.

which can be easily identified by higher or lower density than that of the bulk. The appearance of the edge density profile is favorable for the experimental detection of the bosonic SPT phases.

The rest of this paper is organized as follows. In Sec. II we introduce the target model. In Sec. III we analytically show the quantization of the Z_4 Berry phase by the $Z_2^* \times Z_2^*$ equivalence. In Sec. IV we numerically investigate the presence of the SPT phases in the model. In Sec. V we study the system with an open boundary and numerically investigate the presence of the edge state corresponding to the SPT phase in the bulk. We observe the presence of the edge state where the bulk of the system is in the $Z_2 \times Z_2$ SPT phase. Section VI provides a summary and a brief discussion of prospective study.

II. MODEL

We consider a Bose-Hubbard model on two-leg ladder as shown in Fig. 1. We start by considering the bosonic operator b_{j_x,j_y} with periodic or open boundary condition with

$$\begin{aligned} j_x &\equiv \tfrac{1}{2}, \tfrac{3}{2} \ldots, L-\tfrac{1}{2}, \quad \mod L \text{ (even)}, \\ j_y &\equiv -\tfrac{1}{2}, \tfrac{1}{2}, \quad \mod 2. \end{aligned} \tag{1}$$

The Hamiltonian with the periodic boundary condition is given by (see Fig. 1)

$$H_{\rm BHM} = \sum_{j=0}^{L/2-1} (H_j + H_{j,\rm int}), \tag{2}$$

where.

$$H_j = H_j^{\square} + H_j^{\rm site}, \tag{3}$$

$$H_j^{\square} = -J_v^1 b^\dagger_{2j-1/2,-1/2} b_{2j-1/2,+1/2} - J_v^2 b^\dagger_{2j+1/2,+1/2} b_{2j+1/2,-1/2} - J_h^1 b^\dagger_{2j+1/2,-1/2} b_{2j-1/2,-1/2} - J_h^2 b^\dagger_{2j-1/2,+1/2} b_{2j+1/2,+1/2} + \text{H.c.}, \tag{4}$$

$$H_j^{\rm site} = \sum_{j_x=2j\pm1/2} \left[\left(\sum_{j_y=\pm1/2} \frac{U}{2} n_{j_x,j_y}(n_{j_x,j_y}-1) - \mu n_{j_x,j_y} \right) + \frac{U_{\rm in}}{2} n_{j_x,+1/2} n_{j_x,-1/2} \right], \tag{5}$$

$$H_{j,\rm int} = -J_{\rm int} \sum_{j_y=\pm1/2} b^\dagger_{2j-1/2,j_y} b_{2(j+1)-1/2,j_y} + \text{H.c.}, \tag{6}$$

where $n_{j_x,j_y} = b^\dagger_{j_x,j_y} b_{j_x,j_y}$; L is the ladder length; H_j is a Hamiltonian at the jth plaquette and $J_{\rm int}$ connects them; $J_v^1, J_v^2, J_h^1, J_h^2 \in \mathbb{R}$ are hopping amplitudes as shown in Fig. 1; μ is a chemical potential; U is the on-site interaction (between the same internal states); and $U_{\rm in}$ represents interactions between the upper and lower chains. If the upper and lower chains are created by a different internal state, the atom is in a realistic experimental situation such as a synthetic ladder optical lattice [2,3]. The $U_{\rm in}$ term can be regarded as an interaction between different internal states and the $J_v^{1,2}$ hopping is Rabi coupling. Note that without the synthetic ladder the target system is also feasible in a real experimental system; such a bosonic plaquette optical lattice [33,34] and also a model with synthetic gauge fields have been studied theoretically [35,36]. In what follows, we set $U = U_{\rm in}$ and $\mu = U/2$ and a mean density $\bar{n} = \frac{1}{2L}\sum_{j_x,j_y}\langle n_{j_x,j_y}\rangle$ is used to specify the filling of the system. In most of our work, we focus on a strongly correlated regime $|U| > |J_h^{1(2)}|, |J_v^{1(2)}|, |J_{\rm int}|$, practically $U = 20$, and consider soft-core bosons, where we expect that the ground state is always unique-gapped and also no spontaneous symmetry breaking occurs.

III. SYMMETRY PROTECTION AND FRACTIONAL QUANTIZATION Z_4 BERRY PHASE

We introduce a $Z_2^* \times Z_2^*$ equivalence of the Berry phases associated with $Z_2 \times Z_2$ symmetry (two reflections) of the ladder due to the hopping pattern and the form of the interaction. This $Z_2 \times Z_2$ symmetry can be employed to define a specific type of SPT phases. We then introduce a Berry phase by setting local twists on links. This $Z_2^* \times Z_2^*$ equivalence leads to the Z_4 fractional quantization of the Berry phase.

In what follows, we will explain the $Z_2^* \times Z_2^*$ equivalence and introduce the Z_4 Berry phase. The physical origin of the Z_4 quantization is special for the ladder compared with the previous studies [18–31].

A. $Z_2 \times Z_2$ symmetry

The symmetry constraint to protect a SPT phase we discuss is a combination of two reflections with time reversal. We consider two unitary operators U_x and U_y for reflections shown

in Fig. 1,

$$U_x H_{\rm BHM} U_x^\dagger = U_y H_{\rm BHM} U_y^\dagger = H_{\rm BHM}, \tag{7}$$

where two unitary operators U_x and U_y operate for the boson operators as

$$\begin{aligned} U_x b_{j_x,j_y} U_x^\dagger &= b_{-j_x,j_y}, \quad U_x^2 = 1, \\ U_y b_{j_x,j_y} U_y^\dagger &= b_{j_x,-j_y}, \quad U_y^2 = 1. \end{aligned} \tag{8}$$

Note that this symmetry protection is respected for the periodic boundary condition and also the open boundary condition by cutting the link at the origin [$J_h = 0$ at the $(-\frac{1}{2}, \pm\frac{1}{2})$-$(+\frac{1}{2}, \pm\frac{1}{2})$ link]. It can guarantee the bulk-edge correspondence associated with Z_4 Berry phase as discussed later.

B. Quantized Berry phase as a topological local order parameter

Let us introduce the quantized Berry phase for a generic system by introducing a set of local twists as a parameter set. This type of quantized Berry phase is a topological order parameter of the short-range entangled state [18,19,21,23,28,37]. The generic strategy is as follows. By introduction of the local twists as a set of parameters for the Hamiltonian, the Berry phase is defined for a many-body ground state. Although the Berry phase may take any value generically, one may impose symmetry constraints (with the twists), which induces quantization of the Berry phase. Due to the quantization, this quantized Berry phase cannot be modified by a small but finite perturbation. This implies that the quantized Berry phase is topologically stable and works as a local topological order parameter of the bulk. Since we need an energy gap between the ground state (or set of ground states as a multiplet) and the other states, this topological order parameter is only well defined for the gapped ground state. It picks up responses of the many-body ground state to the local twists as perturbation. If the system is adiabatically modified (without gap closing) and decoupled into a set of local clusters, the system is short-range entangled. Since introduction of a local gauge transformation of the bosonic, fermionic, or spin operators inside some specific cluster does not affect the other clusters and induces twists only inside, it characterizes the locality. Using the twists, a Berry phase of the cluster can be defined assuming the ground state of the cluster is unique. Apparently, it is also considered as a Berry phase of the total system (although the cluster is decoupled). Also, its value is easily evaluated since the twists are gauged out (an example is given below). Using the same twists, even with finite intercluster coupling, one may define a Berry phase associated with the many-body ground state. Note that the twists with finite intercluster coupling cannot be gauge out. In general, this Berry phase may take any value in modulo 2π. However, due to symmetries the system possesses with the twists, the Berry phase may need to satisfy several constraints, which may result in the quantization. This is the quantized Berry phase and then it works as a topological order parameter of the system. Especially when the intercluster coupling is finite but weak enough, this quantized Berry phase is a topological order parameter of the short-range entangle state.

C. Z_4 fractionalization of the ladder

Following this strategy, let us define the Z_4 Berry phase for the periodic boundary condition by introducing a set of four twists $\Theta = (\theta_1, \theta_2, \theta_3, \theta_4)$ only in the plaquette at the origin ($j = 0$) as shown in Figs. 1 and 2. The modified Θ-dependent Hamiltonian $H_{\rm BHM}(\Theta)$ is given by replacing $H_0^\square \to H_0^\square(\Theta)$,

$$\begin{aligned} H_0^\square(\Theta) = &-J_v^1 e^{-i\theta_1} b_2^\dagger b_1 - J_h^1 e^{-i\theta_2} b_3^\dagger b_2 \\ &- J_v^2 e^{-i\theta_3} b_4^\dagger b_3 - J_h^2 e^{-i\theta_4} b_1^\dagger b_4 + \text{H.c.}, \end{aligned} \tag{9}$$

where $b_1 = b_{-1/2,+1/2}$, $b_2 = b_{-1/2,-1/2}$, $b_3 = b_{+1/2,-1/2}$, and $b_4 = b_{+1/2,+1/2}$.

By imposing a constraint $\theta_1 + \theta_2 + \theta_3 + \theta_4 \equiv 0 \,(\text{mod} 2\pi)$, this set of twists is specified by the point in the 3-torus, $T^3 = \{(\theta_1, \theta_2, \theta_3, \theta_4) \mid \theta_1 + \theta_2 + \theta_3 + \theta_4 \equiv 0,\ \theta_i \in \mathbb{R},\ \text{mod} 2\pi\}$, as shown in Fig. 3. We use this extended notation using four parameters to specify the 3-torus, which is useful to discuss the Z_4 symmetry of the ladder (discussed below).

Identifying the equivalent points, any path connecting the vertices P_i ($i = 0, 1, 2, 3$) defines loops ℓ as shown in Fig. 3. Then assuming the ground state is unique (the gap remains open) on the loop, the Berry phase is defined as

$$i\gamma_\ell = \int_\ell \langle\psi | d\psi\rangle \equiv \int_{s_i}^{s_f} ds \langle\psi(s)| \frac{d}{ds} |\psi(s)\rangle, \tag{10}$$

where $|\psi(\Theta)\rangle$ is a ground state of $H_{\rm BHM}(\Theta)$ [$H_{\rm BHM}(\Theta)|\psi(\Theta)\rangle = |\psi(\Theta)\rangle E(\Theta)$] and s is any parameter that specifies the loop, $\ell = \{\Theta(s) \mid s \in [s_i, s_f]\}$. The Z_4 Berry phase ℓ_α is defined by four special paths as

$$\begin{aligned} \ell_{0G1} &= \overrightarrow{P_0 G} + \overrightarrow{G P_1}, \\ \ell_{1G2} &= \overrightarrow{P_1 G} + \overrightarrow{G P_2}, \\ \ell_{2G3} &= \overrightarrow{P_2 G} + \overrightarrow{G P_3}, \\ \ell_{3G0} &= \overrightarrow{P_3 G} + \overrightarrow{G P_0}, \end{aligned} \tag{11}$$

where

$$\begin{aligned} \overrightarrow{P_0 G} &= \left\{ (\theta, \theta, \theta, -3\theta) \,\middle|\, \theta \in \left(0, \frac{2\pi}{4}\right) \right\}, \\ \overrightarrow{P_1 G} &= \left\{ (-3\theta, \theta, \theta, \theta) \,\middle|\, \theta \in \left(0, \frac{2\pi}{4}\right) \right\}, \\ \overrightarrow{P_2 G} &= \left\{ (\theta, -3\theta, \theta, \theta) \,\middle|\, \theta \in \left(0, \frac{2\pi}{4}\right) \right\}, \\ \overrightarrow{P_3 G} &= \left\{ (\theta, \theta, -3\theta, \theta) \,\middle|\, \theta \in \left(0, \frac{2\pi}{4}\right) \right\}. \end{aligned} \tag{12}$$

As for the twisted Hamiltonian, the reflections U_x and U_y, which make the untwisted Hamiltonian invariant, operate as (see Fig. 2)

$$\begin{aligned} &U_x H_{\rm BHM}(\theta_1, \theta_2, \theta_3, \theta_4; J_v^1, J_v^2, J_h^1, J_h^2) U_x^{-1} \\ &\quad = H_{\rm BHM}(-\theta_3, -\theta_2, -\theta_1, -\theta_4; J_v^2, J_v^1, J_h^1, J_h^2), \\ &U_y H_{\rm BHM}(\theta_1, \theta_2, \theta_3, \theta_4; J_v^1, J_v^2, J_h^1, J_h^2) U_y^{-1} \\ &\quad = H_{\rm BHM}(-\theta_1, -\theta_4, -\theta_3, -\theta_2; J_v^1, J_v^2, J_h^2, J_h^1), \end{aligned} \tag{13}$$

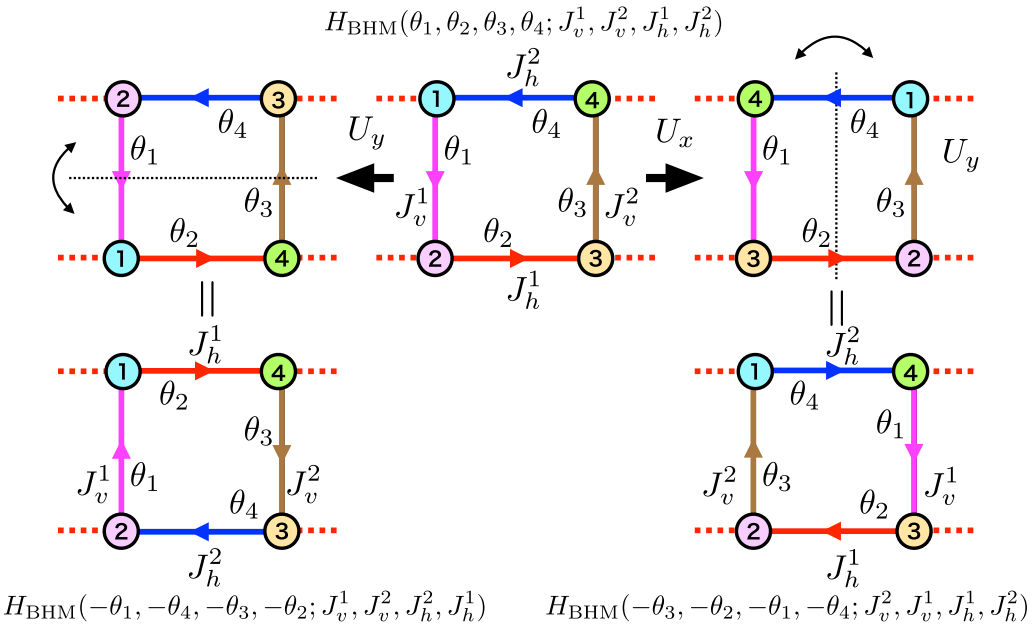

FIG. 2. Two reflections for the Hamiltonian $H_{\rm BHM}$ after introducing the twists in a single plaquette at $j=0$.

where the relevant parameter dependence is explicitly shown. If $J_v^1=J_v^2$, the twisted Hamiltonian on the loop is mapped as

$$\begin{aligned}
\Xi_x H_{\rm BHM}(\Theta)|_{\overrightarrow{P_0G}}\Xi_x^{-1} &= H_{\rm BHM}|_{\overrightarrow{P_0G}}(\Theta),\\
\Xi_x H_{\rm BHM}(\Theta)|_{\overrightarrow{P_1G}}\Xi_x^{-1} &= H_{\rm BHM}|_{\overrightarrow{P_3G}}(\Theta),\\
\Xi_x H_{\rm BHM}(\Theta)|_{\overrightarrow{P_2G}}\Xi_x^{-1} &= H_{\rm BHM}|_{\overrightarrow{P_2G}}(\Theta),\\
\Xi_x H_{\rm BHM}(\Theta)|_{\overrightarrow{P_3G}}\Xi_x^{-1} &= H_{\rm BHM}|_{\overrightarrow{P_1G}}(\Theta),
\end{aligned}\tag{14}$$

where

$$\Xi_x = U_x K, \quad \Xi_y = U_y K, \tag{15}$$

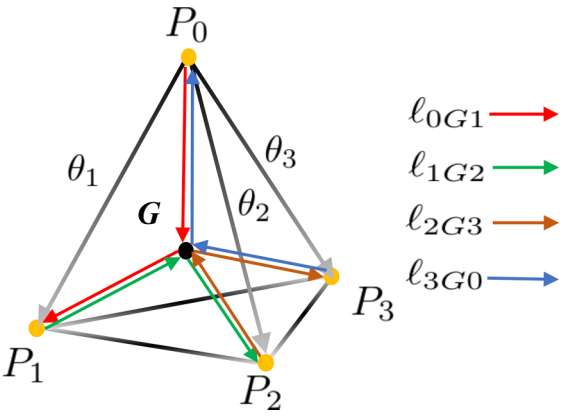

FIG. 3. Three-dimensional parameter space in which to define the Z_4 Berry phases. By using an extended notation, the point in the space is specified by $(\theta_1,\theta_2,\theta_3,\theta_4)$, where $\theta_1+\theta_2+\theta_3+\theta_4\equiv 0 \pmod{2\pi}$, $P_0=(0,0,0,0)$, $P_1=(2\pi,0,0,-2\pi)$, $P_2=(0,2\pi,0,-2\pi)$, $P_3=(0,0,2\pi,-2\pi)$, and $G=(2\pi/4,2\pi/4,2\pi/4,2\pi/4)$. Identifying the equivalent points P_0, P_1, P_2, and P_3, this is a 3-torus T^3.

which implies

$$\begin{aligned}
\Xi_x H_{\rm BHM}(\Theta)|_{\ell_{0G1}}\Xi_x^{-1} &= H_{\rm BHM}|_{\ell_{0G3}}(\Theta),\\
\Xi_x H_{\rm BHM}(\Theta)|_{\ell_{1G2}}\Xi_x^{-1} &= H_{\rm BHM}|_{\ell_{3G2}}(\Theta),\\
\Xi_x H_{\rm BHM}(\Theta)|_{\ell_{2G3}}\Xi_x^{-1} &= H_{\rm BHM}|_{\ell_{2G1}}(\Theta),\\
\Xi_x H_{\rm BHM}(\Theta)|_{\ell_{3G0}}\Xi_x^{-1} &= H_{\rm BHM}|_{\ell_{1G0}}(\Theta).
\end{aligned}\tag{16}$$

Note that, in general, as for the parameter-independent antiunitary operator $\Xi=UK$, where $UU^\dagger=1$, the Berry connection of the state $|\psi^\Xi\rangle=\Xi|\psi\rangle$ is $\langle\psi^\Xi|d\psi^\Xi\rangle=-\langle\psi|d\psi\rangle$ since $\langle\psi|d\psi\rangle$ is pure imaginary. Then using the abbreviations $\gamma_0\equiv\gamma_{\ell_{0G1}}$, $\gamma_1\equiv\gamma_{\ell_{1G2}}$, $\gamma_2\equiv\gamma_{\ell_{2G3}}$, and $\gamma_3\equiv\gamma_{\ell_{3G0}}$, we further write

$$\begin{aligned}
-\gamma_0 &\equiv \gamma_0+\gamma_1+\gamma_2,\\
-\gamma_1 &\equiv -\gamma_2,\\
-\gamma_2 &\equiv -\gamma_1,\\
-\gamma_3 &\equiv -\gamma_0.
\end{aligned}\tag{17}$$

By using the apparent relation $\gamma_0+\gamma_1+\gamma_2+\gamma_3\equiv 0 \bmod 2\pi$ due to the cancellation of the four paths, the relations above are summarized as

$$\gamma_0\equiv\gamma_3, \tag{18}$$

$$\gamma_1\equiv\gamma_2. \tag{19}$$

This naturally implies a partial quantization

$$\gamma_i+\gamma_j=0,\pi \quad (\mathrm{mod}2\pi) \tag{20}$$

for any $i\neq j$ except $(i,j)=(0,3),(1,2)$.

Similarly, if $J_h^1=J_h^2$, we have the relations

$$\begin{aligned}
\Xi_y H_{\rm BHM}(\Theta)|_{\overrightarrow{P_0G}}\Xi_y^{-1} &= H_{\rm BHM}|_{\overrightarrow{P_2G}}(\Theta),\\
\Xi_y H_{\rm BHM}(\Theta)|_{\overrightarrow{P_1G}}\Xi_y^{-1} &= H_{\rm BHM}|_{\overrightarrow{P_1G}}(\Theta),\\
\Xi_y H_{\rm BHM}(\Theta)|_{\overrightarrow{P_2G}}\Xi_y^{-1} &= H_{\rm BHM}|_{\overrightarrow{P_0G}}(\Theta),\\
\Xi_y H_{\rm BHM}(\Theta)|_{\overrightarrow{P_3G}}\Xi_y^{-1} &= H_{\rm BHM}|_{\overrightarrow{P_3G}}(\Theta).
\end{aligned}\tag{21}$$

This implies

$$\begin{aligned}
\Xi_y H_{\rm BHM}(\Theta)|_{\ell_{0G1}} \Xi_y^{-1} &= H_{\rm BHM}|_{\ell_{2G1}}(\Theta),\\
\Xi_y H_{\rm BHM}(\Theta)|_{\ell_{1G2}} \Xi_y^{-1} &= H_{\rm BHM}|_{\ell_{1G0}}(\Theta),\\
\Xi_y H_{\rm BHM}(\Theta)|_{\ell_{2G3}} \Xi_y^{-1} &= H_{\rm BHM}|_{\ell_{0G3}}(\Theta),\\
\Xi_y H_{\rm BHM}(\Theta)|_{\ell_{3G0}} \Xi_y^{-1} &= H_{\rm BHM}|_{\ell_{3G2}}(\Theta)
\end{aligned} \tag{22}$$

and then

$$\begin{aligned}
-\gamma_0 &\equiv -\gamma_1,\\
-\gamma_1 &\equiv -\gamma_0,\\
-\gamma_2 &\equiv \gamma_0+\gamma_1+\gamma_2 \equiv -\gamma_3,\\
-\gamma_3 &\equiv -\gamma_2,
\end{aligned} \tag{23}$$

which are summarized as

$$\gamma_0 \equiv \gamma_1, \tag{24}$$

$$\gamma_2 \equiv \gamma_3. \tag{25}$$

This naturally implies a partial quantization

$$\gamma_i + \gamma_j = 0, \pi \pmod{2\pi} \tag{26}$$

for any $i \neq j$ except $(i, j) = (0, 1), (2, 3)$.

If the ladder satisfies the full $Z_2 \times Z_2$ symmetries, $J_v^1 = J_v^2$ and $J_h^1 = J_h^2$, supplemented with the constraint $\gamma_0 + \gamma_1 + \gamma_2 + \gamma_3 = 0$,

$$\gamma_0 \equiv \gamma_1 \equiv \gamma_2 \equiv \gamma_3 = 2\pi\frac{n}{4}, \quad n \in \mathbb{Z} \pmod{2\pi}. \tag{27}$$

This is the Z_4 quantization of the ladder. We call it the Z_4 Berry phase [21,32].

D. Plaquette limit

The quantized values (20), (26), and (27) are fixed explicitly if the system is adiabatically connected to a set of decoupled plaquettes ($J_{\rm int} = 0$). As for the Z_4 Berry phase, it is enough to consider a single plaquette in this case. The twists Θ are gauged out (or they are induced) by the gauge transformation [see Eq. (9)]

$$H_{\rm BHM}(\Theta) = U_\Theta H_{\rm BHM} U_\Theta^{-1} \quad \text{if } J_{\rm int} = 0, \tag{28}$$

$$U_\Theta = e^{-i\phi_1 n_1} e^{-i\phi_2 n_2} e^{-i\phi_3 n_3} e^{-i\phi_4 n_4}, \tag{29}$$

where $U_\Theta b_j U_\Theta^\dagger = e^{+i\phi_j} b_j$ $(j = 1, 2, 3, 4)$, $\phi_1(\Theta) = 0$, $\phi_2(\Theta) = \theta_1$, $\phi_3(\Theta) = \theta_1 + \theta_2$, and $\phi_4(\Theta) = \theta_1 + \theta_2 + \theta_3$, which implies that $|\psi(\Theta)\rangle = U_\Theta|\psi(0)\rangle$. Noting that $[n_i, U_\Theta] = 0$, the Berry connection and the Berry phase are given as

$$\langle\psi|d\psi\rangle = \langle\psi(0)|U_\Theta^\dagger dU_\Theta|\psi(0)\rangle = -i\sum_{i=1}^{4} d\phi_i \langle n_i\rangle_0,$$

$$\gamma_\ell = -i\int_\ell \langle\psi|d\psi\rangle = \sum_i \langle n_i\rangle_0 \Delta\phi_i, \tag{30}$$

where $\langle n_i\rangle_0 = \langle\psi(0)|n_i|\psi(0)\rangle$ and $\Delta\phi_i = \phi_i(\Theta(s))|_{s_i}^{s_f}$. As for the canonical loops, we have

$$\begin{aligned}
\gamma_0 &= -2\pi(\langle n_2\rangle_0 + \langle n_3\rangle_0 + \langle n_4\rangle_0),\\
\gamma_1 &= 2\pi\langle n_2\rangle_0,\\
\gamma_2 &= 2\pi\langle n_3\rangle_0,\\
\gamma_3 &= 2\pi\langle n_4\rangle_0.
\end{aligned} \tag{31}$$

We assume that the ground state of the total system (and thus that of the plaquette as well) is unique. Then the total number of bosons in the plaquette is a positive integer $M = \sum_{i=1}^4 \langle n_i\rangle_0$.

When $J_v^1 = J_v^2$, due to the Z_2 invariance by U_x, $\langle n_1\rangle_0 = \langle n_4\rangle_0$ and $\langle n_2\rangle_0 = \langle n_3\rangle_0$. This implies

$$\begin{aligned}
\gamma_0 &= -2\pi(M - \langle n_1\rangle_0) \equiv 2\pi\langle n_1\rangle_0\\
&= 2\pi\langle n_4\rangle_0 = \gamma_3 \pmod{2\pi},\\
\gamma_1 &= \gamma_2.
\end{aligned} \tag{32}$$

Also, due to this Z_2, $\langle n_1\rangle_0 + \langle n_2\rangle_0 = \langle n_3\rangle_0 + \langle n_4\rangle_0 = M/2$, which implies the partial quantization

$$\gamma_0 + \gamma_1 \equiv \gamma_2 + \gamma_3 \equiv \frac{M}{2} \pmod{2\pi}. \tag{33}$$

Similarly, when $J_h^1 = J_h^2$, due to the Z_2 invariance by U_y, $\langle n_1\rangle_0 = \langle n_2\rangle_0$ and $\langle n_3\rangle_0 = \langle n_4\rangle_0$. This implies

$$\begin{aligned}
\gamma_0 &= -2\pi(M - \langle n_1\rangle_0) \equiv 2\pi\langle n_1\rangle_0\\
&= 2\pi\langle n_2\rangle_0 = \gamma_1 \pmod{2\pi},\\
\gamma_2 &= \gamma_3.
\end{aligned} \tag{34}$$

Also $\langle n_1\rangle_0 + \langle n_4\rangle_0 = \langle n_2\rangle_0 + \langle n_3\rangle_0 = M/2$, which implies the partial quantization

$$\gamma_0 + \gamma_3 \equiv \gamma_1 + \gamma_2 \equiv \frac{M}{2} \pmod{2\pi}. \tag{35}$$

Then when the system is $Z_2 \times Z_2$ invariant, $J_v^1 = J_v^2$ and $J_h^1 = J_h^2$ and we have the Z_4 quantization

$$\gamma_0 \equiv \gamma_1 \equiv \gamma_2 \equiv \gamma_3 \equiv \frac{M}{4} \pmod{2\pi}. \tag{36}$$

These quantized Berry phases are adiabatic invariants.

E. Another Z_2 Berry phase

We also consider a set of twists in H_0 by assuming the Z_2 symmetry due to U_x, that is, $J_v^1 = J_v^2 = J_v$ as

$$\begin{aligned}
H_0^\square(\theta) = &-J_v b_2^\dagger b_1 - J_h^1 e^{-i\theta} b_3^\dagger b_2\\
&- J_v b_4^\dagger b_3 - J_h^2 e^{-i\theta} b_1^\dagger b_4 + \text{H.c.}
\end{aligned} \tag{37}$$

We also consider a Berry phase γ^{Z_2} associated with this set of twists. Due to the Z_2 symmetry, it is quantized into Z_2 as

$$\gamma^{Z_2} \equiv 0, \pi \pmod{2\pi}. \tag{38}$$

This is due to the symmetry constraint

$$\gamma^{Z_2} \equiv -\gamma^{Z_2}. \tag{39}$$

A dimer limit ($J_v^1 = J_v^2 = 0, J_{\rm int} = 0$) is the decoupled limit for this case:

$$H_{\rm BHM}(\theta) = U_\theta H_{\rm BHM} U_\theta^{-1} \quad \text{if } J_v = J_{\rm int} = 0, \tag{40}$$

$$U_\theta = e^{-i\theta n_1} e^{-i\theta n_3}. \tag{41}$$

In this decoupled case,

$$\langle\psi|d\psi\rangle = \langle\psi(0)|U_\theta^\dagger dU_\theta|\psi(0)\rangle = -id\theta(\langle n_1\rangle_0 + \langle n_3\rangle_0),$$
$$\gamma^{Z_2} = -i\int_\ell \langle\psi|d\psi\rangle = 2\pi(\langle n_1\rangle_0 + \langle n_3\rangle_0). \tag{42}$$

Further, $\langle n_1\rangle_0 = \langle n_4\rangle_0$ and $\langle n_2\rangle_0 = \langle n_3\rangle_0$ due to the Z_2 invariance by U_x. This implies $\langle n_1\rangle_0 + \langle n_3\rangle_0 = \langle n_2\rangle_4 + \langle n_3\rangle_0 = M/2$. Then adiabatic continuation to this dimer limit guarantees

$$\gamma^{Z_2} \equiv 2\pi\frac{M}{2} \equiv \pi M \quad (\mathrm{mod}2\pi). \tag{43}$$

IV. NUMERICAL EVALUATION OF THE Z_4 SPT PHASE

In the preceding section we showed the Z_4 fractional quantization of the Z_4 Berry phase by the $Z_2 \times Z_2$ symmetry. We now turn to the numerical demonstration of its fractional quantization in the Hamiltonian H_{BHM} by using diagonalization [38] for various parameter conditions. In the numerical calculation of the Z_4 Berry phase, we employed a discrete formula shown in Appendix A. The numerical procedure of the Z_4 Berry phase is efficient since it gives a quantized value even if the discretization step is not so small. The characterization of the topological phase by the quantized quantities works well, as expected from previous works [18–32]. The fractional quantization of the Z_4 Berry phase signals the presence of the bulk SPT phase protected by the $Z_2 \times Z_2$ symmetry.

In what follows, we set $J_v^1 = J_v^2 = J_v$ and $J_h^1 = J_h^2 = J_h$. We introduce a dimerization parameter δJ as $J_{\mathrm{int}} = 1 - \delta J$, with $J_h = \delta J$, and set $J_v = 1$. This setting preserves the $Z_2 \times Z_2$ symmetry. We focus on $U = 20$ and consider soft-core bosons.

Varying δJ for $\bar{n} = 0.25$, 0.5, and 0.75, the Z_4 Berry phase behaves as shown in Fig. 4(a). For $\delta J > 0.5$ and $\bar{n} = 0.25$ and 0.75, we observe the fractional quantizations $\gamma_0/2\pi = \frac{1}{4}$ and $\frac{3}{4}$ and the Z_4 Berry phase captures clear topological phase transitions at $\delta J = 0.5$. On the other hand, for $\bar{n} = 0.5$, the finite fractional quantization $\gamma_0/2\pi = \frac{2}{4}$ appears even for a finite δJ. The reason is that two dimer states residing on J_v links on a plaquette are adiabatically connected to a plaquette cluster state. These results of the fractional quantization signal the presence of the bulk SPT phases of the $Z_2 \times Z_2$ symmetry. Also note that the quantization value of the Z_4 Berry phase is related to the mean density $\gamma_0/2\pi = \bar{n}$, which is expected when considering a decoupled plaquette limit.

We then calculate the Z_2 Berry phase. Since the model of H_{BHM} has inversion symmetry, the Z_2 Berry phase can capture a topological phase transition from $\gamma^{Z_2} = 0$ to $\gamma^{Z_2} = \pi$ [23]. Figure 4(b) shows the behavior of the Z_2 Berry phase. We observe that for the $\bar{n} = 0.25$ and 0.75 cases, the Z_2 Berry phase characterizes a topological phase transition and its topological phase, but for $\bar{n} = 0.5$ the Z_2 Berry phase does not capture the presence of the bulk SPT phase.

We observe the effects of the interaction U. The Z_4 Berry phase exhibits an interesting behavior for $\bar{n} = 0.75$, as shown in Fig. 4(c). While varying δJ we observe an intermediate plateau phase with $\gamma_0/2\pi = \frac{1}{2}$ for a moderate U and δJ; this behavior is specific to the bosonic system [39,40]. This intermediate phase we find is interesting in that this state is not adiabatically connected to the state of the plaquette limit, which exhibits the $\gamma_0/2\pi = \frac{3}{4}$ state.

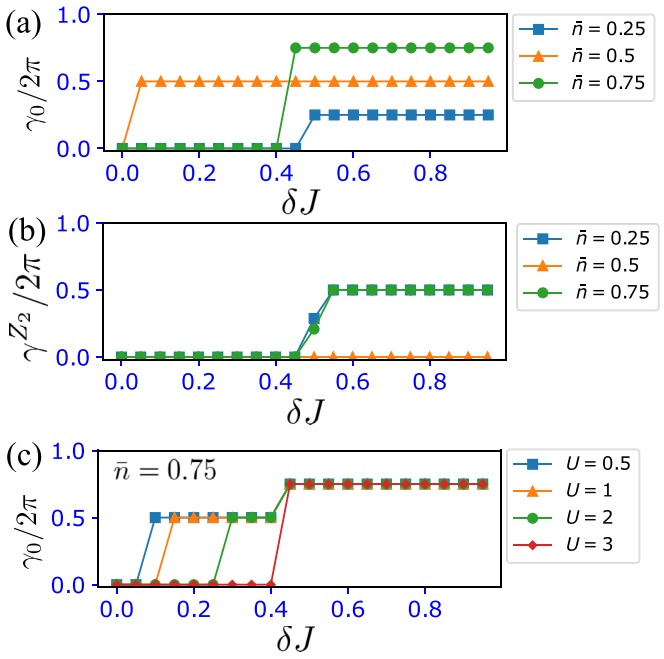

FIG. 4. (a) Behavior of the Z_4 Berry phase for various mean densities with $U = 20$. (b) Behavior of the Z_2 Berry phase for various mean densities with $U = 20$. (c) Behavior of the Z_4 Berry phase for various U with $\bar{n} = 0.75$. In the numerical diagonalization, the maximum occupation number of the boson on a site is truncated up to 4. For $U \ll 1$, a superfluid phase appears where the gap is very small and the value of the Berry phase is unstable. For all data, we set $L = 8$.

Next, while introducing the notion of the SPT phase it is important to focus on the symmetry of the system. In this work the $Z_2 \times Z_2$ symmetry is of our interest. If some system's parameter varies with the symmetry intact, we expect the SPT phase is robust. This reflects the robustness of the quantization of the Z_4 Berry phase. Inversely, without or breaking the symmetry in the system by some perturbation, the SPT phase protected by $Z_2 \times Z_2$ symmetry no longer appears. We verify it numerically. To observe the importance of the $Z_2 \times Z_2$ symmetry for the presence of the SPT phase, we introduce here a symmetry-breaking potential (a similar numerical observation exists in [25]). As a perturbation, we add a potential

$$V_p = V_0 \sum_{j=0}^{L/2-1} (n_{2j-1/2,-1/2} + n_{2j+1/2,+1/2}), \tag{44}$$

which breaks the $Z_2 \times Z_2$ symmetry. We expect that as V_0 increases, the fractional quantization of the Z_4 Berry phase collapses. In fact, we verify this expectation as shown in Fig. 5. For each density $\bar{n}$, the quantization continuously breaks down with increasing V_0. This result indicates that the $Z_2 \times Z_2$ symmetry is crucial for the existence of the SPT phase in the bosonic system.

An interesting behavior of the Z_4 Berry phase in the system with *only* U_x symmetry is observed (U_y is broken). From Eqs. (18) and (19), a certain relation of the Z_4 Berry phase

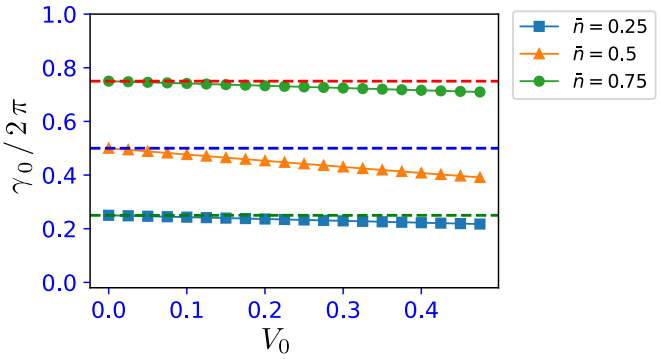

FIG. 5. Effect of the perturbation breaking the $Z_2 \times Z_2$ symmetry. We set $\delta J = 0.8$ and $U = 20$. The red, blue, and green dashed lines represent the ideal quantization values $\gamma_0/2\pi = \frac{1}{4}, \frac{2}{4}$, and $\frac{3}{4}$, respectively. For all data, we set $L = 8$.

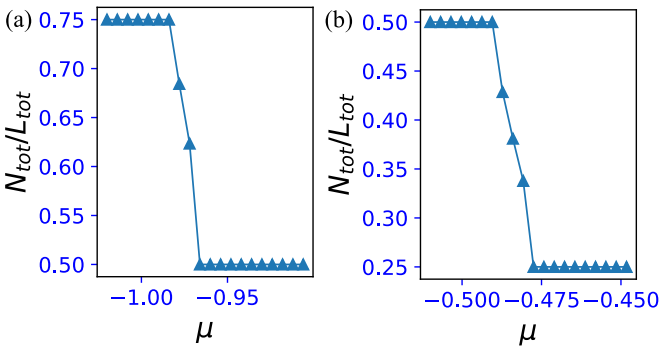

FIG. 7. The μ dependence of the total density in the system with the periodic boundary condition. The total number of the lattice site is $L_{\rm tot} = 2L = 64$ ($L = 32$) and $N_{\rm tot}$ is the total particle number. We set $J_{\rm int} = 0.1$, $J_h = 0.9$, and $U = 20$.

exists,

$$\gamma_0 + \gamma_1 = \gamma_2 + \gamma_3. \tag{45}$$

Combined with the relation $\sum_\alpha \gamma_\alpha = 0 \ (\mathrm{mod} 2\pi)$, we obtain

$$\begin{aligned} \gamma_0 + \gamma_1 &= 0, \pi \quad (\mathrm{mod} 2\pi), \\ \gamma_2 + \gamma_3 &= 0, \pi \quad (\mathrm{mod} 2\pi). \end{aligned} \tag{46}$$

The sum of the two Z_4 Berry phases is quantized. We verify this unconventional quantization. To this end, we modify the parameters $J_{\rm int}$ and J_h as

$$J_{\rm int} \to \begin{cases} 1 - \delta J \equiv J^2_{\rm int} & \text{(upper chain)} \\ 1 - (\delta J - 0.1) \equiv J^1_{\rm int} & \text{(lower chain)}, \end{cases} \tag{47}$$

$$J^2_h = \delta J, \quad J^1_h = \delta J - 0.1. \tag{48}$$

The Hamiltonian $H_{\rm BHM}$ is no longer invariant for the Z_2 symmetry U_y and invariant only for the Z_2 symmetry U_x. For $\bar{n} = 0.25$, we demonstrate the quantization of the sum of the Z_4 Berry phases. Figure 6 is the numerical result. Depending on the value of δJ, the sum $\gamma_0 + \gamma_1$ takes a value of 0 or π and we observe a clear phase transition, while both γ_0 and γ_1 take some fractional values for any δJ or do not take the value of $2\pi/4$. Hence, we confirm the Z_2 quantization of the sum of the Z_4 Berry phase as shown in Eq. (46).

In addition, we expect that the bulk SPT phases appear in the spinless free-fermion system. In Appendix B we confirm

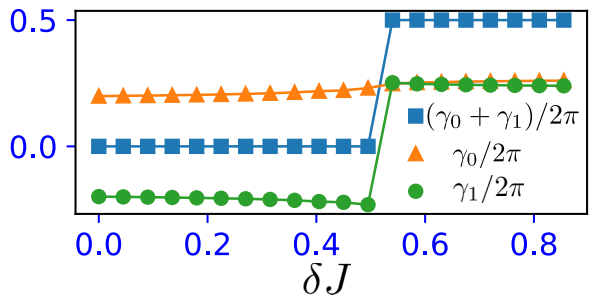

FIG. 6. The δJ dependence of the Z_4 Berry phase in the system with only U_x symmetry. Even for $\delta J > 0.4$, $\gamma_0/2\pi$ and $\gamma_1/2\pi \neq \frac{1}{4}$. For all data we set the interaction as $U = 20$ and $L = 8$.

the presence of the SPT phase, which is also characterized by the fractional quantization of the Z_4 Berry phase.

Before going to the next section, we show the DMRG calculation allowing the change of the particle number in the system to consolidate the presence of the bulk SPT phases as shown in Fig. 5(a). We employ the DMRG algorithm by using the TeNPy library [41]. In the calculation, we vary the chemical potential μ in the system with the periodic boundary condition. The total number of lattice sites is $L_{\rm tot} = 2L$ and the total particle number is denoted by $N_{\rm tot}$. In the DMRG calculation throughout this work, we take the bond dimension to be 80–120, truncate the singular values less than 10^{-4} in the update of the matrix product state, and set the convergence condition of the ground-state energy, $\Delta E < 10^{-5} J_v$. The results are shown in Fig. 7, for the same parameters as in Fig. 4(a). We find some plateaus with the total particle number constant. The results indicate that the density on each plateau corresponds to that of each bulk SPT phase as shown in Figs. 7(a) and 7(b); each state on each plateau is gapped and incompressible. This is reminiscent of the appearance of the magnetization plateaus [23,42] and the density plateaus of the Mott insulator in the conventional Bose-Hubbard model [43].

V. EDGE STATES IN BOSONIC SPT PHASES

In general, the bulk-edge correspondence is to read out the information of the bulk from various edge states for various forms of the edge. Conversely, if a nontrivial bulk state exists, then one introduces an edge in the system and some edge state appears. It is possible to predict the form of the edge state from inferring what states appear by cutting the decoupled plaquette in this system.

For the bosonic system in this work, if we believe the presence of the bulk-edge correspondence, some bosonic edge state can appear for some edge shape. However, it is difficult to directly deduce the presence and detailed properties of the edge state since the bosonic system we are considering is complex due to the ladder geometry, the presence of the interactions, the vertical hoppings, and the soft-core boson nature. It is difficult to identify some symmetries that would characterize the appearance of edge states as they appear in free fermions (cf. chiral symmetry). Even in this situation,

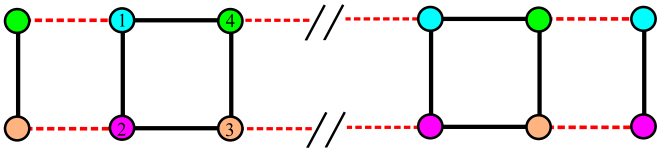

FIG. 8. Schematic image of the introduction of a vertical edge. This open boundary system is invariant under both U_x and U_y

when we set an experimentally feasible edge shape of interest, we can confirm at least numerically, on a case-by-case, what edge states appear. Thus, we perform such a study in the following.

To detect some edge state, we also employ the DMRG algorithm [41]. We impose here an open boundary condition and analyze two cases: a vertical edge case and a diagonal edge case. For both cases, we employ the simulation allowing the change of particle number in the system (grand-canonical ensemble), that is, we vary the chemical potential μ and observe density properties of both bulk and edges. We expect that edge states (if they appear) are different from those of a conventional free-fermion system with a certain topological phase. In particular, we note that, in general, bosonic systems with an open boundary do not necessarily have a zero-energy edge state, e.g., due to the lack of chiral symmetry. This has already been reported in interacting bosonic systems and numerically verified in the context of the topological Mott insulator [44] and Haldane insulator [45].

A. Vertical edge case

We first focus on the system with a vertical edge as shown in Fig. 8. The edge is simply introduced by cutting a single plaquette at $j = 0$ in the periodic system. The boundary preserves both U_x and U_y symmetries.

We start by observing the behavior of the total density $N_{\rm tot}$ obtained by summing over the local density of all sites with varying μ. The total number of lattice sites is $L_{\rm tot} = 2L$. The result is shown in Figs. 9(a) and 9(b). We observe how the behavior of the total density of the periodic case as shown in Fig. 7 changes by introducing edges. Like for the periodic boundary calculations in Fig. 7, we find some plateaus with the total density constant. For each plateau, the bulk states correspond to the bulk SPT phases with a different Z_4 Berry phase

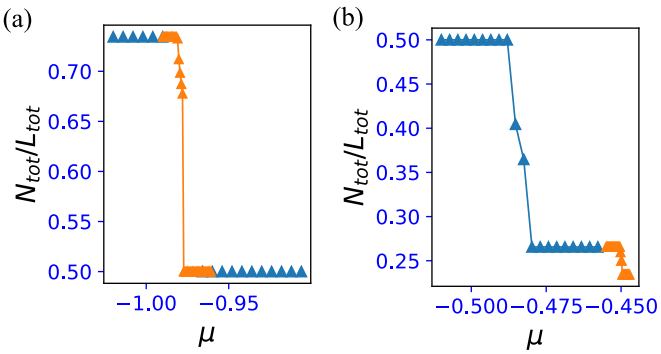

FIG. 9. The μ dependence of the total density $N_{\rm tot}/L_{\rm tot}$. Here $L_{\rm tot} = 2L = 64$ ($L = 32$). We set $J_{\rm int} = 0.1$ and $J_h = 0.9$.

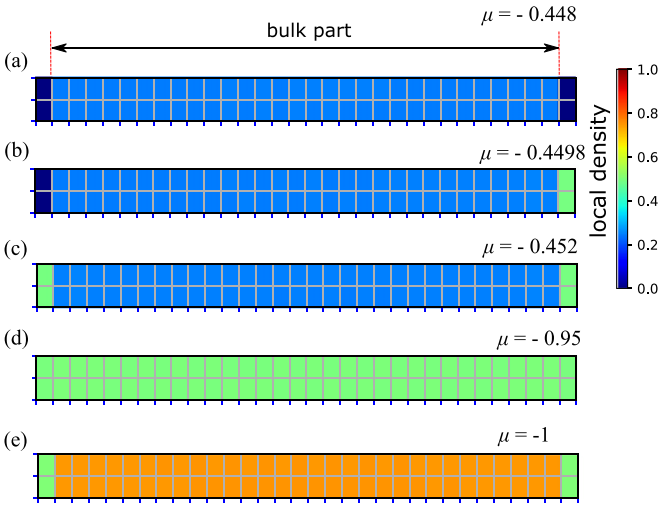

FIG. 10. Density distribution under the diagonal edge for (a) $\mu = -0.448$, (b) $\mu = -0.44498$, (c) $\mu = -0.452$, (d) $\mu = -0.95$, and (e) $\mu = -1$. In the data of (d), the edge state is created on the left and right edge sites. The bulk part includes $L_{\rm tot} - 4$ sites (here we set $L = 32$).

(the density distribution will be shown later). Interestingly, we find two more small plateau regimes around $\mu = -0.45$, where the particle distribution on the edges is specific, as shown later.

Now we study the local density distribution for specific μ's on each plateau and what type of edge state appears. The distribution at $\mu = -0.448$ in the rightmost small plateau in Fig. 9(b) is shown in Fig. 10(a). The bulk part has $\bar{n} = 0.25$, corresponding to the phase with $\gamma_\alpha/2\pi = \frac{1}{4}$, and the left and right edge sites appear empty (localized holes). No bosonic edge state appears. Next we focus on the $\mu = -0.4498$ case; this point is in the second (very) small plateau from the right in Fig. 9(b). As shown in Fig. 10(b), we find here that a localized edge state at the right edge sites appears. This state is close to a single bonding state forming on the rung of a ladder,[1] $\frac{1}{\sqrt{2}}[b_1^\dagger + b_2^\dagger]$. The bulk SPT phase with $\gamma_\alpha/2\pi = \frac{1}{4}$ remains. Specifically, the whole of the wave function can be written as $|\psi^R(\mu = -0.4498)\rangle \sim \frac{1}{\sqrt{2}}[b_{1,R}^\dagger + b_{2,R}^\dagger]|{\rm bulk}\rangle$, where $|{\rm bulk}\rangle$ is the bulk SPT state. This edge state is expected from the decoupled plaquette limit for $\bar{n} = 0.25$. If we cut the single plaquette into two halves, some bondinglike states can appear. Also, we expect that at $\mu = -0.4498$, the ground state is twofold degenerate, that is, the state $|\psi^L(\mu = -0.4498)\rangle \sim \frac{1}{\sqrt{2}}[b_{3,L}^\dagger + b_{4,L}^\dagger]|{\rm bulk}\rangle$ is also another ground state. Here, in practice, our DMRG calculation chooses just the right edge state $|\psi^R(\mu = -0.4498)\rangle$. In fact, note that, due to the presence of degenerate states, the true observed local density is obtained as $\langle n_j\rangle = {\rm Tr}(\rho_{gs} n_j)$, where $\rho_{gs} = \frac{1}{2}[|\psi^R(\mu = -0.4498)\rangle\langle\psi^R(\mu = -0.4498)| +$

[1]Strictly, the edge state is not a strict bonding state due to small $J_{\rm int}$, $\frac{1}{\sqrt{2}}[b^\dagger + b^\dagger]$. However, our numerical result shows that the edge state is much close to the bonding state. Thus, we call such a close state an edge state in this section.

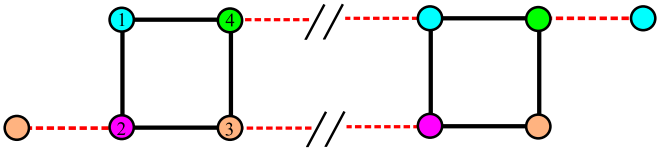

FIG. 11. Schematic image of a diagonal edge. We set $|J_h| \gg |J_{\rm int}|$. This open boundary system is invariant under U_xU_y and not invariant under the individual U_x and U_y. The total number of lattice sites of the system is $L_{\rm tot} = 2L + 2$.

$|\psi^L(\mu = -0.4498)\rangle\langle\psi^L(\mu = -0.4498)|]$. Then the densities of the left and right edge sites are all the same, i.e., 0.25.

We next show in Fig. 10(c) the distribution at $\mu = -0.452$ in the third plateau from the right in Fig. 9(b). There, at both edges, the localized edge states appear. Varying μ induces the additional appearance of the edge state. The bulk SPT phase remains. The state is $|\psi(\mu = -0.452)\rangle \sim \frac{1}{2}[b^\dagger_{3,L} + b^\dagger_{4,L}][b^\dagger_{1,R} + b^\dagger_{2,R}]|\text{bulk}\rangle$.

We further show the smaller μ case. The distribution at $\mu = -0.495$ in the leftmost plateau in Fig. 9(b) is shown in Fig. 10(d). The bulk state changes to $\bar{n} = 0.5$, corresponding to the SPT phase with $\gamma_\alpha/2\pi = \frac{2}{4}$, and remains the edge state at both edges. The state is $|\psi(\mu = -0.452)\rangle \sim \frac{1}{2}[b^\dagger_{3,L} + b^\dagger_{4,L}][b^\dagger_{1,R} + b^\dagger_{2,R}]|\text{bulk}\rangle$, where $|\text{bulk}\rangle$ is the SPT phase with $\bar{n} = 0.5$. This numerical result indicates that for the change of μ around the plateau jumps, $\mu \sim -0.48$, the bulk state changes rather than the edge state. We expect that the reason is a large density fluctuation due to the bosonic nature. It is difficult to find some types of edge states expected from the decoupled plaquette limit for $\bar{n} = 0.5$, compared to the low-density region.

Finally, we observe in Fig. 10(e) the distribution at $\mu = -1$ in the left plateau in Fig. 9(a). The bulk part has $\bar{n} = 0.75$, corresponding to the phase with $\gamma_\alpha/2\pi = \frac{3}{4}$. As in the previous case shown in Fig. 10(d), the single edge state remains at both edges. The state is $|\psi(\mu = -1)\rangle \sim \frac{1}{2}[b^\dagger_{3,L} + b^\dagger_{4,L}][b^\dagger_{1,R} + b^\dagger_{2,R}]|\text{bulk}\rangle$, where $|\text{bulk}\rangle$ is the SPT phase with $\bar{n} = 0.75$. From this result, the bulk state tends to change rather than the edge state around the plateau jumps ($\mu \sim -0.98$).

Summarizing the results of the vertical edge case, we observe that the appearance of the edge state close to the bonding state, identified by the difference in density from that of the bulk (mean density $\bar{n}$), depends on the Z_4 SPT phase in the bulk with different mean density $\bar{n}$. In particular, for the bulk SPT phase with $\gamma_\alpha/2\pi = \frac{1}{4}$, some types of edge state appear by fine-tuning μ. These states are predicted from the state of the decoupled plaquette limit.

B. Diagonal edge case

We now study the diagonal edge case. The shape of the edges is shown in Fig. 11. Note that this edge geometry cannot be obtained by a periodic ladder ring as in the vertical edge shown in Fig. 8, but is obtained by cutting an infinite ladder. Here the length of the bulk part is L and the total number of lattice sites is $L_{\rm tot} = 2L + 2$. In contrast to the vertical edge case, the boundary condition breaks individual U_x and

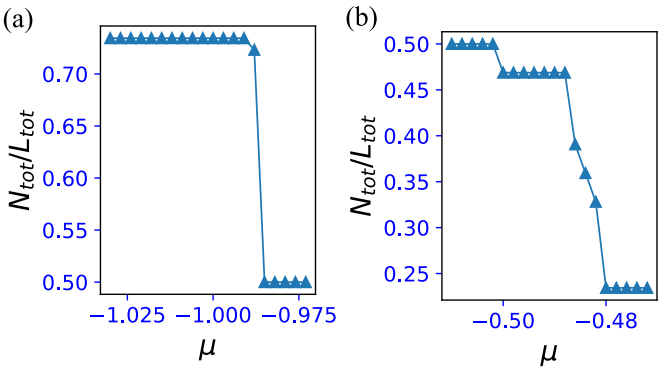

FIG. 12. The μ dependence of the total density $N_{\rm tot}/L_{\rm tot}$. Here $L_{\rm tot} = 2L + 2 = 62$ ($L = 30$). We set $J_{\rm int} = 0.1$ and $J_h = 0.9$.

U_y symmetries, but the $U_x \times U_y$ symmetry remains. We focus on the density distribution for each single site for the case $|J_h| > |J_{\rm int}|$ and numerically investigate whether some edge states appear. For the diagonal edge, the sites on the edges do not couple to another site in the vertical direction, that is, there are no vertical hopping and interactions, implying that a localized particle edge state or hole around the edges can appear.

We start by observing the behavior of the total density $N_{\rm tot}$ obtained by summing over the local density of all sites with varying μ. The result is shown in Figs. 12(a) and 12(b). Like the calculations of the periodic boundary condition in Fig. 7, we find some plateaus with the total density constant. For each plateau the bulk states correspond to the bulk SPT phases with a different Z_4 Berry phase. Interestingly, we find one more plateau around $\mu = -0.49$, where the particle distribution on the edges is specific, as shown later.

We further show some local density distributions for specific μ's on each plateau. The distribution at $\mu = -0.47$ in the rightmost plateau in Fig. 12(b) is shown in Fig. 13(a). The bulk part has $\bar{n} = 0.25$, corresponding to the phase with $\gamma_\alpha/2\pi = \frac{1}{4}$, and a single hole appears at the left and right edge sites. A localized particle edge state does not appear.

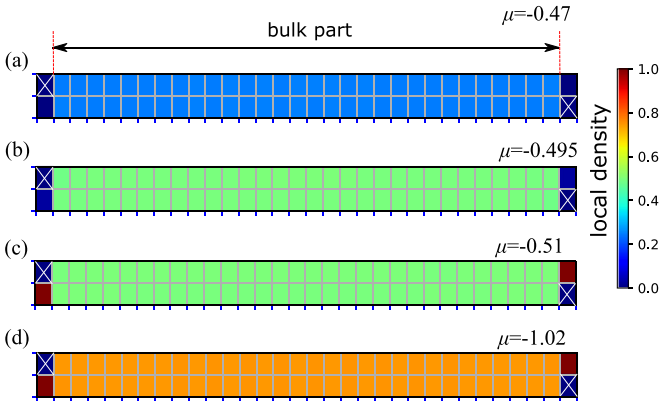

FIG. 13. Density distribution under the diagonal edge for (a) $\mu = -0.47$, (b) $\mu = -0.495$, (c) $\mu = -0.51$, and (d) $\mu = -1.02$. The white cross represents a site where the particle occupation is not prohibited due to the diagonal edges. The bulk part includes $2L$ sites (here we set $L = 30$).

The reason is that if such a particle exists for finite $J_{\rm int}$, the particle tends to intrude on the bulk part due to the low density, but once the particle enters the bulk (which is likely to occur due to the low density of the bulk), the state is energetically unstable due to the presence of interactions. Next we show in Fig. 13(b) the distribution at $\mu = -0.495$ in the middle plateau in Fig. 12(b). The bulk part has $\bar{n} = 0.5$, corresponding to the phase with $\gamma_\alpha/2\pi = \frac{2}{4}$, and we observe a single hole at the left and right edge sites. However, upon a little decrease in μ, this plateau is swept and another plateau appears. See the distribution at $\mu = -0.51$ shown in Fig. 13(c). The bulk SPT state remains the same as the case of Fig. 13(b). Interestingly, a localized particle edge state appears at the left and right edge sites, which are greatly localized at the edge sites. Further, note that the localized particle edge state can be a gapless localized particle since the gap between the leftmost and middle plateaus in Fig. 13(b) is $1/L$ and for $L \to \infty$, the gap is closed.

Finally, we observe in Fig. 13(d) the distribution at $\mu = -1.02$ in the left plateau in Fig. 12(a). The bulk part has $\bar{n} = 0.75$, corresponding to the phase with $\gamma_\alpha/2\pi = \frac{3}{4}$, and interestingly a localized particle edge state appears at the left and right edge sites. No hole appears at the edges between the rightmost and middle plateaus as shown in Fig. 13(b).

Summarizing the results of the diagonal edge case, some particle edge state greatly localized on the single edge site appears by fine-tuning μ. In general, the presence of interactions reveals unconventional behaviors of the particle density around the edges. However, on some stable plateaus, we numerically find the presence of clear localized particle edge states, where the local density in the bulk takes a specific constant related to the value of the Z_4 Berry phase.

The presence of the localized particle edge state can be identified as a higher value of density than that of the bulk. Finally, we comment that the local density distributions including edge sites for both the vertical and diagonal edge cases presented in this section are observable in real experiments since a recent experimental technique using a quantum gas microscope can take a snapshot of the local density in an optical lattice and has already identified the presence of edge states from the density profile [46].

VI. CONCLUSION

We have proposed a concrete example of interacting SPT phases defined by $Z_2 \times Z_2$ symmetry in a Bose-Hubbard model on a two-leg ladder. The system considered in this work is feasible for real experiments such as cold atoms in an optical lattice. We showed that the $Z_2 \times Z_2$ symmetry coming from the lattice geometry leads to a fractional quantization of the Z_4 Berry phase. The Z_4 Berry phase acts as an efficient topological order parameter for the interacting bosonic system. We numerically demonstrated the presence of the bosonic bulk Z_4 SPT phases characterized by the fractional quantization of the Z_4 Berry phase. The phase structure is rich depending on the boson density and strength of interaction, etc. Based on the expectation of the presence of the bulk-edge correspondence, we investigated whether or not some edge states appear for two cases by using the DMRG calculation allowing the change of particle number (grand-canonical ensemble): the vertical edge case and the diagonal edge case. In the vertical edge case, we observed the appearance of the edge state close to the bonding state by fine-tuning μ. In particular, for the bulk SPT phase with $\gamma_\alpha/2\pi = \frac{1}{4}$, some types of edge states appear by fine-tuning μ. These states are predicted from the state of the decoupled plaquette limit. In the diagonal edge case, some particle edge states greatly localized on the single edge site appear by fine-tuning μ, where the bulk states is of course the SPT phase.

As a future direction of study it would be interesting to extend the ladder geometry to a two-dimensional lattice and to investigate whether some higher-order topological phase [28,47–49] exists based on this $Z_2 \times Z_2$ type of symmetry. Finally, even though we focused on the Z_4 Berry phase throughout this work, it would be interesting to consider additional symmetry-breaking terms with time dependence. Then Berry curvature based on this Z_4 Berry phase can be introduced and may lead to some source of topological pumping. This issue would be important.

ACKNOWLEDGMENTS

The work was supported by JSPS KAKEN-HI through Grants No. 21K13849 (Y.K.), No. 23K13026 (Y.K.), and No. 23H01091 (Y.H.) and JST CREST(Japan) through Grant No. JPMJCR19T1 (Y.H.).

APPENDIX A: DISCRETE VERSION OF Eq. (10)

To calculate Eq. (10) numerically, we employ a discrete formulation, often used in the numerical calculation for the Z_2 Berry phase and Chern number [50]. The discretized version of Eq. (10) is given as

$$\gamma_\ell = \mathrm{Im} \ln \prod_{k=1}^{M} \langle \psi(s_k) | \psi(s_{k+1}) \rangle, \tag{A1}$$

where the parameter s is discretized as $s \to s_k = \Delta s k + s_i$, with $\Delta s = (s_f - s_i)/M$ and $k = 1, \ldots, M$. We take the number of discretization $M = 24$, which is sufficient to observe the stable quantization behavior.

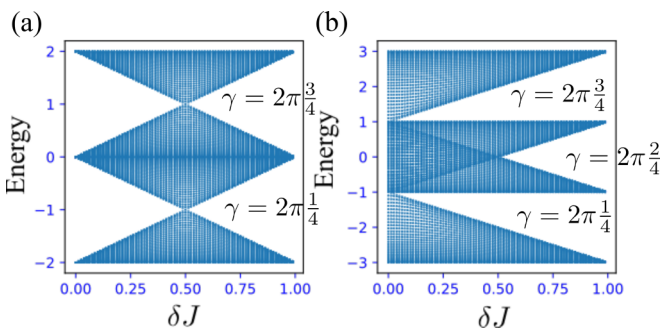

FIG. 14. Single-particle spectrum for (a) $J_h = \delta J$ and $J_{\rm int} = 1 - \delta J$ and (b) $J_h = 1 - \delta J$ and $J_{\rm int} = 1 + \delta J$. For both cases, we set $J_v = 1$.

APPENDIX B: FREE SPINLESS FERMION SYSTEM

The SPT phase protected by the $Z_2 \times Z_2$ symmetry can be defined in a free-spinless-fermion system. We calculate the single-particle spectrum of the system for two different parameter sets of J_1 and J_2 with the periodic boundary condition. The results are shown in Fig. 14. In Fig. 11(a) where we set $J_{\text{int}} = 1 - \delta J$ and $J_h = \delta J$, at $\delta J = 0.5$ the first and second gaps are closed and reopened for $\delta J > 0.5$. When the system's Fermi energy resides in the first gap, the filling is $\frac{1}{4}$ and there we observe the Z_4 Berry phase $\gamma/2\pi = \frac{1}{4}$, while with the Fermi energy in the second gap, the filling is $\frac{3}{4}$ and there we observe the Z_4 Berry phase $\gamma/2\pi = \frac{3}{4}$.

We further show another different parameter set where $J_{\text{int}} = 1 - \delta J$ and $J_h = 1 + \delta J$. The spectrum is shown in Fig. 11(b). We observe that the first and third gaps appear for $\delta J > 0$, while the second gap opens at $\delta J = 0.5$. With the Fermi energy in the first gap, the filling is $\frac{1}{4}$ and there we observe the Z_4 Berry phase $\gamma/2\pi = \frac{1}{4}$; with the Fermi energy in the second gap, the filling is $\frac{2}{4}$ and there we observe the Z_4 Berry phase $\gamma/2\pi = \frac{2}{4}$; and with the Fermi energy in the second gap, the filling is $\frac{3}{4}$ and there we observe the Z_4 Berry phase $\gamma/2\pi = \frac{3}{4}$. From these results, the free-fermion system also exhibits the various SPT phases protected by the $Z_2 \times Z_2$ symmetry.

[1] T. Ozawa, H. M. Price, A. Amo, N. Goldman, M. Hafezi, L. Lu, M. C. Rechtsman, D. Schuster, J. Simon, O. Zilberberg, and I. Carusotto, Rev. Mod. Phys. **91**, 015006 (2019).

[2] M. Mancini, G. Pagano, G. Cappellini, L. Livi, M. Rider, J. Catani, C. Sias, P. Zoller, M. Inguscio, M. Dalmonte, and L. Fallani, Science **349**, 1510 (2015).

[3] B. K. Stuhl, H.-I. Lu, L. M. Aycock, D. Genkina, and I. B. Spielman, Science **349**, 1514 (2015).

[4] J. H. Kang, J. H. Han, and Y. Shin, Phys. Rev. Lett. **121**, 150403 (2018).

[5] J. H. Han, J. H. Kang, and Y. Shin, Phys. Rev. Lett. **122**, 065303 (2019).

[6] J. H. Kang, J. H. Han, and Y. I. Shin, New J. Phys. **22**, 013023 (2020).

[7] J. H. Han, D. Bae, and Y. Shin, Phys. Rev. A **105**, 043306 (2022).

[8] I. Bloch, J. Dalibard, and W. Zwerger, Rev. Mod. Phys. **80**, 885 (2008).

[9] C. Trefzger, C. Menotti, B. Capogrosso-Sansone, and M. Lewenstein, J. Phys. B **44**, 193001 (2011).

[10] S. Baier, M. J. Mark, D. Petter, K. Aikawa, L. Chomaz, Z. Cai, M. Baranov, P. Zoller, and F. Ferlaino, Science **352**, 201 (2016).

[11] F. Pollmann, E. Berg, A. M. Turner, and M. Oshikawa, Phys. Rev. B **85**, 075125 (2012).

[12] A. Altland and M. R. Zirnbauer, Phys. Rev. B **55**, 1142 (1997).

[13] A. Kitaev, in *Proceedings of the Landau Memorial Conference on Advances in Theoretical Physics, Chernogolovka, 2008*, edited by V. Lebedev and M. Feigel'man, AIP Conf. Proc. No. 1134 (AIP, Melville, 2009), pp. 22–30.

[14] S. Ryu, A. P. Schnyder, A. Furusaki, and A. W. W. Ludwig, New J. Phys. **12**, 065010 (2010).

[15] X. Chen, Z.-C. Gu, Z.-X. Liu, and X.-G. Wen, Science **338**, 1604 (2012).

[16] X. Chen, Z. C. Gu, Z. X. Liu, and X. G. Wen, Phys. Rev. B **87**, 155114 (2013).

[17] A. Mazurenko, C. S. Chiu, G. Ji, M. F. Parsons, M. Kanasz-Nagy, R. Schmidt, F. Grusdt, E. Demler, D. Greif, and M. Greiner, Nature (London) **545**, 462 (2017).

[18] Y. Hatsugai, J. Phys. Soc. Jpn. **75**, 123601 (2006).

[19] T. Hirano, H. Katsura, and Y. Hatsugai, Phys. Rev. B **77**, 094431 (2008).

[20] I. Maruyama, T. Hirano, and Y. Hatsugai, Phys. Rev. B **79**, 115107 (2009).

[21] Y. Hatsugai and I. Maruyama, Europhys. Lett. **95**, 20003 (2011).

[22] N. Chepiga, F. Michaud, and F. Mila, Phys. Rev. B **88**, 184418 (2013).

[23] T. Kariyado and Y. Hatsugai, Phys. Rev. B **91**, 214410 (2015).

[24] I. Maruyama and S. Miyahara, J. Phys. Soc. Jpn. **87**, 123703 (2018).

[25] T. Kariyado, T. Morimoto, and Y. Hatsugai, Phys. Rev. Lett. **120**, 247202 (2018).

[26] T. Kawarabayashi, K. Ishii, and Y. Hatsugai, J. Phys. Soc. Jpn. **88**, 045001 (2019).

[27] T. Mizoguchi, H. Araki, and Y. Hatsugai, J. Phys. Soc. Jpn. **88**, 104703 (2019).

[28] H. Araki, T. Mizoguchi, and Y. Hatsugai, Phys. Rev. Res. **2**, 012009(R) (2020).

[29] Y. Kuno and Y. Hatsugai, Phys. Rev. B **104**, 125146 (2021).

[30] Y. Otsuka, T. Yoshida, K. Kudo, S. Yunoki, and Y. Hatsugai, Sci. Rep. **11**, 20270 (2021).

[31] M. Bunney, T. Mizoguchi, Y. Hatsugai, and S. Rachel, Phys. Rev. B **105**, 045113 (2022).

[32] Y. Hatsugai and Y. Kuno, Phys. Rev. B **107**, 235106 (2023).

[33] B. Paredes and I. Bloch, Phys. Rev. A **77**, 023603 (2008).

[34] S. Nascimbène, Y.-A. Chen, M. Atala, M. Aidelsburger, S. Trotzky, B. Paredes, and I. Bloch, Phys. Rev. Lett. **108**, 205301 (2012).

[35] M. Buser, C. Hubig, U. Schollwöck, L. Tarruell, and F. Heidrich-Meisner, Phys. Rev. A **102**, 053314 (2020).

[36] S. Greschner, M. Piraud, F. Heidrich-Meisner, I. P. McCulloch, U. Schollwöck, and T. Vekua, Phys. Rev. A **94**, 063628 (2016).

[37] T. Kariyado and Y. Hatsugai, Phys. Rev. B **90**, 085132 (2014).

[38] P. Weinberg and M. Bukov, SciPost Phys. **7**, 020 (2019); **2**, 003 (2017).

[39] X. Deng and L. Santos, Phys. Rev. A **89**, 033632 (2014).

[40] Y. Kuno, K. Shimizu, and I. Ichinose, New J. Phys. **19**, 123025 (2017).

[41] J. Hauschild and F. Pollmann, SciPost Phys. Lect. Notes **5**, 1 (2018).

[42] M. Oshikawa, M. Yamanaka, and I. Affleck, Phys. Rev. Lett. **78**, 1984 (1997).

[43] M. P. A. Fisher, P. B. Weichman, G. Grinstein, and D. S. Fisher, Phys. Rev. B **40**, 546 (1989).

[44] F. Grusdt, M. Höning, and M. Fleischhauer, Phys. Rev. Lett. **110**, 260405 (2013).
[45] S. Stumper and J. Okamoto, Phys. Rev. A **101**, 063626 (2020).
[46] P. Sompet, S. Hirthe, D. Bourgund, T. Chalopin, J. Bibo, J. Koepsell, P. Bojović, R. Verresen, F. Pollmann, G. Salomon, C. Gross, T. A. Hilker, and I. Bloch, Nature (London) **606**, 484 (2022).
[47] W. A. Benalcazar, B. A. Bernevig, and T. L. Hughes, Phys. Rev. B **96**, 245115 (2017).
[48] Y. You, J. Bibo, and F. Pollmann, Phys. Rev. Res. **2**, 033192 (2020).
[49] D. González-Cuadra, Phys. Rev. B **105**, L020403 (2022).
[50] T. Fukui, Y. Hatsugai, and H. Suzuki, J. Phys. Soc. Jpn. **74**, 1674 (2005).